JOURNAL OF SYNCHROTRON RADIATION
ISSN 1600-5775

Characterization of a quadrant diamond transmission X-ray detector including a precise determination of the mean electron–hole pair creation energy

Jeffrey W. Keister,[a]* Levent Cibik,[b] Swenja Schreiber[b] and Michael Krumrey[b]

[a]NSLS-II, Brookhaven National Laboratory, Upton, NY 11973-5000, USA, and [b]Physikalisch-Technische Bundesanstalt (PTB), Abbestrasse 2-12, 10587 Berlin, Germany. *Correspondence e-mail: jkeister@bnl.gov

Received 28 July 2017
Accepted 10 December 2017

Edited by Y. Amemiya, University of Tokyo, Japan

Keywords: X-ray; detectors; diamond; calibration; scattering; quadrant diamond transmission X-ray detector.

Precise monitoring of the incoming photon flux is crucial for many experiments using synchrotron radiation. For photon energies above a few keV, thin semiconductor photodiodes can be operated in transmission for this purpose. Diamond is a particularly attractive material as a result of its low absorption. The responsivity of a state-of-the art diamond quadrant transmission detector has been determined, with relative uncertainties below 1% by direct calibration against an electrical substitution radiometer. From these data and the measured transmittance, the thickness of the involved layers as well as the mean electron–hole pair creation energy were determined, the latter with an unprecedented relative uncertainty of 1%. The linearity and X-ray scattering properties of the device are also described.

1. Introduction

For many experiments using X-rays, and in particular those using monochromatized synchrotron radiation, the incident photon flux must be known or at least relative flux variations must be recorded. For this purpose, detectors for flux monitoring are required. In the ideal case, these detectors are permanently installed in the incoming beam. In the photon energy range above several keV, very thin semiconductor photodiodes are well suited as they are small, easy to operate and do not require cooling (Krumrey *et al.*, 2007). Because of its low absorption, diamond is a particularly attractive material for these transmission X-ray detectors (TXDs).

If responsivity and transmittance of a TXD have been determined with low uncertainties, not only the incident photon flux, but also the transmitted photon flux arriving at the experiment can be calculated. Furthermore, the properties of the detector itself can be deduced. The main parameters are the thicknesses of the involved layers (the semiconductor material as well as the front and back contacts) and the mean energy for electron–hole pair creation in the semiconductor, w. For diamond, only limited measurements of w have been available so far. For 5.5 MeV alpha particles, a pulse-height ratio of 3.61 ± 0.06 for different diamond samples relative to silicon suggests a w value of (13.1 ± 0.2) eV (Kozlov *et al.*, 1975; Canali *et al.*, 1979). For continuous X-ray beams, several estimates have been published, namely: (i) a value of (13.25 ± 0.50) eV (Keister & Smedley, 2009), consistent with subsequent results (Desjardins *et al.*, 2014), and (ii) a value of (13.05 ± 0.20) eV (Morse *et al.*, 2008). A determination with lower uncertainty, which accounts for incomplete collection efficiency, is presented in this paper.

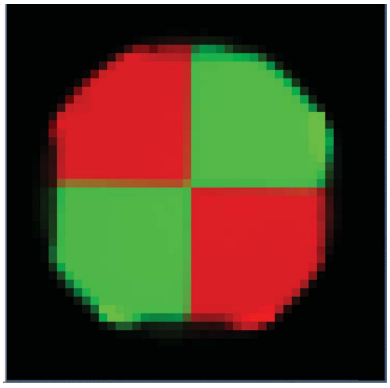

© 2018 International Union of Crystallography

2. Experimental

As diamond material and processing improves towards the state of the art, TXDs of this material have become available. This investigation reports the performance of a commercially available thin, ultrahigh-purity, single-crystal diamond sensor with platinum surface electrodes. Basic features include: <5 parts per billion substitutional nitrogen content, high crystal quality (tested by X-ray topography and visible-light polarimetry), thin plate (∼50 µm or less), and thin (∼30 nm) non-Ohmic platinum contacts, prepared using dead-layer-free surface oxidation pre-treatment (Muller *et al.*, 2014). Platinum is used because of its robustness to oxidation and its ability to form a blocking (Schottky) contact on diamond; this is important for avoiding photoconductive gain which can result from hole injection into the metallization in the event of localized charge trapping in the diamond (Gaowei *et al.*, 2012). Plates are 4 to 4.5 mm square, providing an active area of ∼3 mm diameter. Contact patterning provides measurements of beam position (a quadrant pattern is provided on one surface of the sensor, with a common bias contact on the reverse). The high-purity sensor is non-doped, therefore an applied bias (10 V, providing ∼0.2 MVm^{-1} field) is used to collect a photo-induced charge for an electrical performance similar to silicon photodiodes. The development and demonstration of similar detectors is reported elsewhere (Keister & Smedley, 2009; Berdermann *et al.*, 2010; Muller *et al.*, 2010, 2012; Desjardins *et al.*, 2014).

All measurements of responsivity and transmittance were performed in the laboratory of the Physikalisch-Technische Bundesanstalt (PTB), the German National Metrology institute, at the synchrotron radiation facility BESSY II in Berlin, Germany (Beckhoff *et al.*, 2009). The four-crystal monochromator 'FCM' beamline covers the photon energy range from 1.75 to 10 keV, providing radiation with high spectral purity – total relative higher harmonic power below 10^{-4} (Krumrey & Ulm, 2001). The TXD was placed on an X–Y stage in ultra-high vacuum and electrically connected to a calibrated Keithley 617 Electrometer, which was also used to determine the TXD shunt resistance of 0.4 PΩ; the typical dark current at 10 V operating voltage is ∼25 fA.

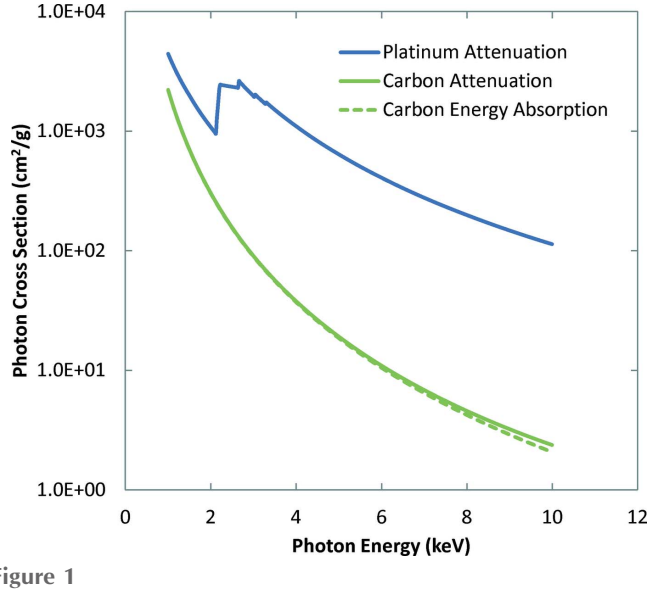

Figure 1
Photon cross sections for platinum (electrical surface contacts) and carbon (diamond sensor) from the literature (Berger *et al.*, 2010; Hubbell & Seltzer, 2004). The Pt *M* absorption edges above 2 keV are clearly visible.

The transmittance was simply obtained by flux measurements using a silicon photodiode with and without the TXD in the beam. Transmission and responsivity were measured simultaneously for each sample location in steps of 5 eV below 3400 eV, and in steps of 100 eV above this photon energy. Representative values for the fitting were collected near the center of one contact, far from contact edges. To obtain the responsivity with the lowest uncertainties, the TXD was directly calibrated against a cryogenic electrical substitution radiometer (Gerlach *et al.*, 2008). This primary detector standard allows the measurement of radiant power in the 10^{-9} to 10^{-4} Watt range, by proven equivalence to electrical heating power, which can easily be determined from electrical measurements.

3. Responsivity and transmission measurements, and analysis

The measurements of the responsivity s and the transmittance T are made within a single element of the quadrant-patterned device to avoid transition areas. The overall model functions, which explicitly take into account the transmission-defined thickness and collection efficiency are:

$$s(E_{\rm Ph}, U) = \varepsilon(E_{\rm Ph}, U)\left(\frac{1}{w}\right)\Big(\exp[-\mu_{\rm Pt}(E_{\rm Ph})t_{\rm Pt\_f}] \times \{1 - \exp[-\mu_{\rm en,dia}(E_{\rm Ph})t_{\rm dia}]\}\Big), \quad (1)$$

$$T(E_{\rm Ph}) = \exp[-\mu_{\rm Pt}(E_{\rm Ph})(t_{\rm Pt\_f} + t_{\rm Pt\_b}) - \mu_{\rm dia}(E_{\rm Ph})t_{\rm dia}], \quad (2)$$

where $E_{\rm Ph}$ is the photon energy; U the applied bias voltage; ε the charge collection efficiency; $t_{\rm Pt\_f}$, $t_{\rm Pt\_b}$ and $t_{\rm dia}$ the thicknesses of the platinum front contact, platinum back contact and the diamond substrate, respectively; $\mu_{\rm Pt}$ and $\mu_{\rm dia}$ the absorption coefficients for platinum and diamond, and $\mu_{\rm en,dia}$ the mass energy-absorption coefficient for diamond (each coefficient μ is the product of the cross section and the density). The photon cross sections shown in Fig. 1 are taken from the XCOM Photon Cross Sections Database (Berger *et al.*, 2010; Hubbell & Seltzer, 2004). It is worth noting that total attenuation of X-rays by diamond exceeds the energy absorption by up to 13% at the highest photon energies used in the study (10 keV), owing to non-absorptive Compton scattering. Both terms are therefore used in the model at all energies. To calculate the absorption coefficients, densities for diamond and platinum are taken as 3.51 and 21.45 g cm^{-3}, respectively.

The photon energy and bias dependent charge collection efficiency ε is determined from bias scans at several representative photon energies. While only a small bias is required

to attain significant response (*e.g.* 1 V yields no less than an 80% relative response for the energies probed here), additional bias continues to increase the responsivity asymptotically. This behavior is well approximated by a bi-exponential function, with an ∼90% or more contribution from the short-range (up to ∼1 V) behavior, and the remainder with an extended range (∼30 V). The long-range contribution is more pronounced for the higher photon energies, as shown in Fig. 2(*a*). The bi-exponential behavior observed is consistent with the model of Hecht for the field-dependent efficiency of electron and hole collection (Hecht, 1932). With positive bias on the exit contact, holes are collected at the entrance, traveling further, on average, at higher photon energies. A fit of these functions reveals the extrapolated value of the ultimate responsivity, to which the responsivity at a nominal bias (*e.g.* 10 V) can be compared.

As we apply a consistent 10 V bias for all subsequent responsivity measurements, the 10 V relative collection efficiency shown in Fig. 2(*b*) is estimated for use at the full range of photon energies by making use of a simple relation:

$$\varepsilon_{10}(E_{\rm Ph}) = \exp\left[-\left(c_{10a}E_{\rm Ph} + c_{10b}{E_{\rm Ph}}^2\right)\right] \qquad (3)$$

where the constants c_{10a} and c_{10b} are coefficients relevant to the 10 V relative efficiency, and fit to the data at the discrete test energies with a relative error of 0.2% or less. The effect of the electric field being insufficient for a full charge collection at a 10 V bias is seen to have a maximum impact of up to 7.9% responsivity reduction at a photon energy of 10 keV. The collection efficiency function accounts for this in the overall responsivity model. We note that this bulk recombination loss, with its characteristic bi-exponential behavior, is consistent with bulk recombination (Almaviva *et al.*, 2010), and distinct from surface recombination (Keister *et al.*, 2010).

The remaining parameters (w, $t_{\rm Pt\_f}$, $t_{\rm Pt\_b}$ and $t_{\rm dia}$) in equations (1) and (2) are obtained by the simultaneous fitting of the measured responsivity and transmission curves using the overall models, with the results shown in Fig. 3. The decreasing transmittance towards lower photon energies is mainly a result

Table 1
Parameter values and uncertainties determined from the simultaneous fitting of the transmission and responsivity data shown in Fig. 3.

Parameter	Fit value and uncertainty estimate
w	12.82 ± 0.13 eV
$t_{\rm Pt\_f}$	141 ± 10 nm
$t_{\rm Pt\_b}$	66 ± 10 nm
$t_{\rm dia}$	45.2 ± 0.6 µm

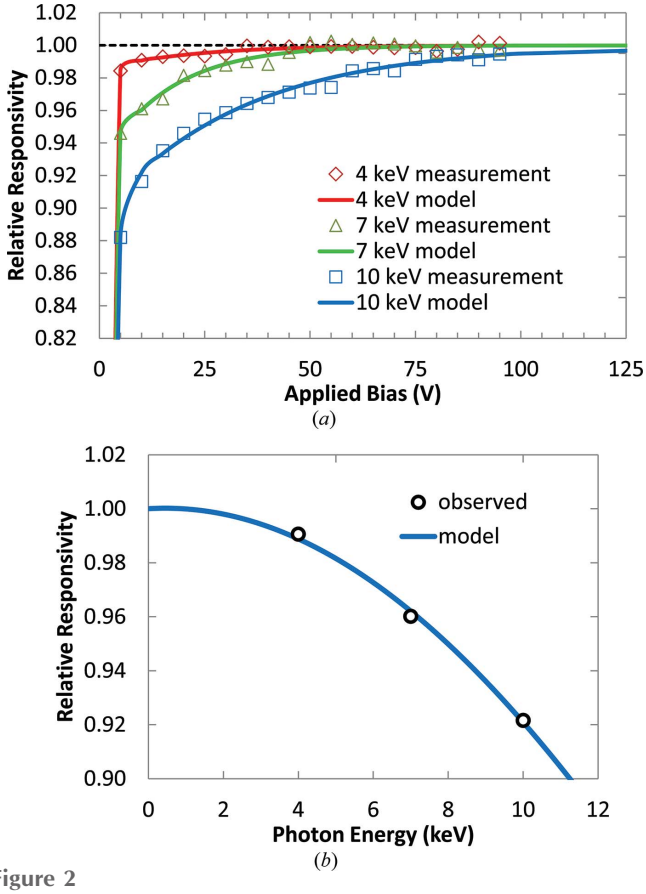

Figure 2
Relative collection efficiency (*a*) as a function of bias for several photon energies, and (*b*) as a function of photon energy at 10 V bias including the model function.

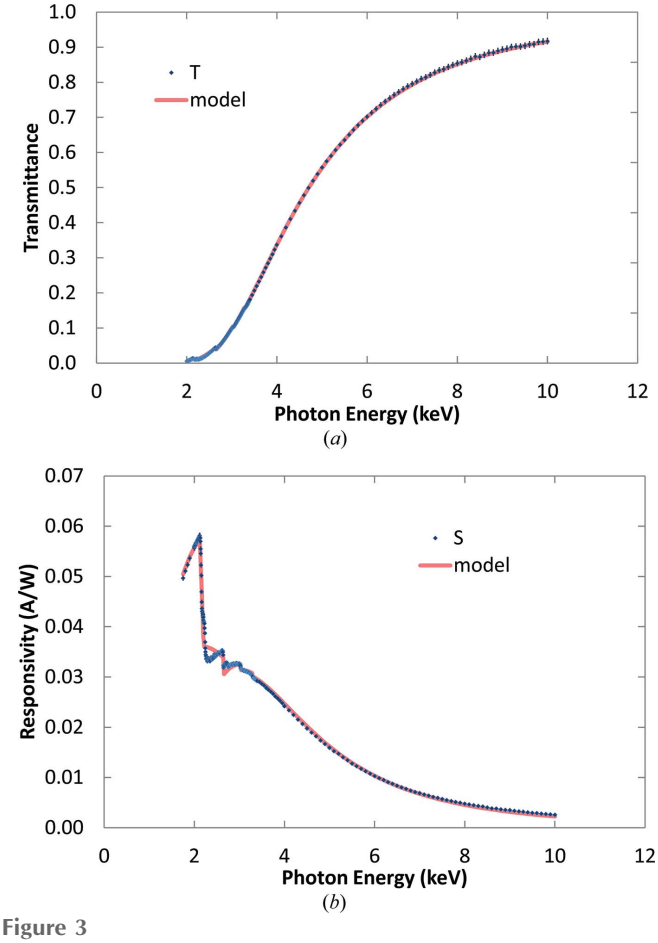

Figure 3
Measured and modeled transmission (*a*) and responsivity (*b*) for the TXD using equations (1) and (2) as well as the collection efficiency according to equation (3).

of absorption in the diamond substrate, while the sharp features in the responsivity above 2 keV are due to the absorption in the Pt front contact. The four parameters obtained from the fit are shown in Table 1.

Uncertainty estimates for the fit parameters are provided for 68% confidence level ($\pm 1\sigma$), obtained from variations applied in a number of ways (offset, slope and random) to the measurements and cross sections. The obtained uncertainty estimates for the fit parameters are limited mainly by the relative uncertainty of $\sim$1% in the measurements, and, to a lesser extent, the $\sim$2% uncertainty in the cross-section data (Hubbell, 1999). The fit parameters refine previous estimates for w as well as laboratory estimates of the relevant thickness values.

4. Spatial uniformity and linearity

An X-ray beam of about 0.1 mm × 0.1 mm was used to probe the spatial uniformity of transmittance and responsivity at different photon energies. The data for 7 keV are shown in Fig. 4.

The transmittance is enhanced at the 38 µm gap or 'street' between adjacent platinum contacts of the quadrant pattern. The effects at the edges are consistent with cropping and/or reflection of the beam by the holder, and possible underfilling of the aperture with the diamond plate. Within the quadrant areas the transmittance is quite uniform, within 1 to 2% over the active surface as seen in Fig. 4(*b*). The responsivity data show a gradual gradient of response, on the order of 3 to 4% over the active surface as seen in Fig. 4(*c*). This feature is also observed at other test photon energies, and may be an indication of the crystal quality; slight degradation near the plate edges can occur during growth or polishing (Muller *et al.*, 2010).

The transmittance enhancement in the gap correlates with increased responsivity at lower photon energies and reduced responsivity at higher photon energies. At lower photon energies, the lack of metal gives a significant increase in absorption, and the charge (generated near the incident surface) is rather efficiently collected, drifting little before significant diffusion can occur. At higher photon energies, the metal thickness is less important to absorption, but the charge is less efficiently collected, having been generated deeper in the diamond, and experiencing a reduced field in the gap between incident electrodes.

The responsivity is expected to be independent of the incident flux. This linearity is tested by a method similar to that provided earlier (Krumrey *et al.*, 2010). In this method, the beamline optics are used to vary the incident flux over several orders of magnitude while the illuminated area varies by less than a factor of two, thus the flux density is truly varied. Good responsivity linearity is observed, with a variability within ±0.5% over two decades of incident power (roughly 0.1 to 10 µW mm^{-2}), at three photon energies, as shown in Fig. 5. Earlier demonstration of linearity for this type of sensor has exceeded six decades, with variability within roughly 20% (Bohon *et al.*, 2010).

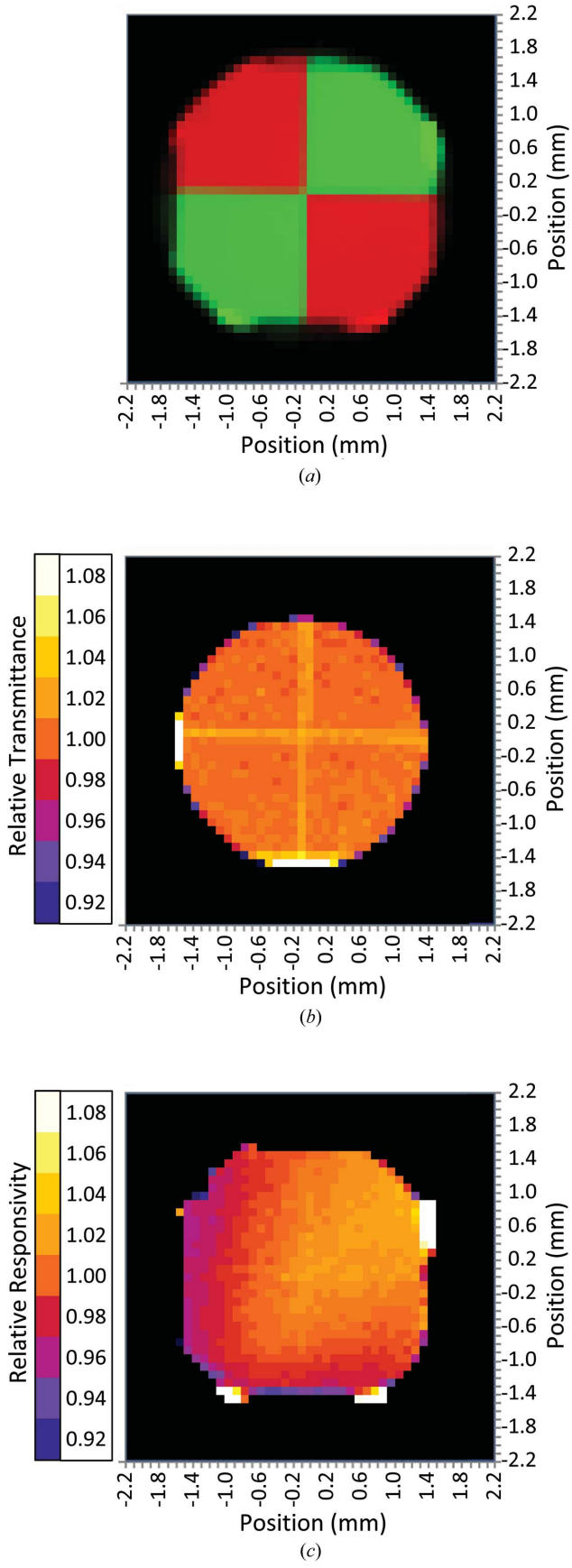

Figure 4
Quadrant structure (*a*), relative transmittance (*b*), and relative responsivity (*c*) at 7 keV photon energy. Details are provided in the text.

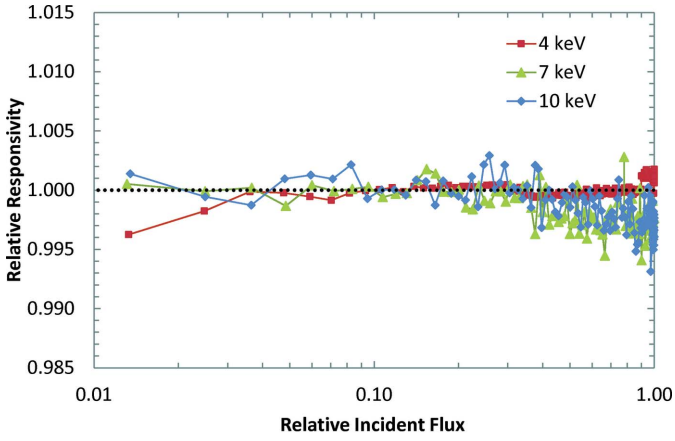

Figure 5
Responsivity variation with power density, in the range of roughtly 0.1 to 10 μW mm^{-2}.

5. Scattering performance

While diffraction artifacts affecting spectroscopy can be dealt with using focusing optics (Ravel *et al.*, 2013), the TXD should not contribute significantly to the scattering background. This is especially important for small-angle X-ray scattering (SAXS) measurements of weakly scattering biological samples (Varga *et al.*, 2014) and for anomalous scattering (ASAXS), where small variations of the scattered intensity close to absorption edges are evaluated (Hoell *et al.*, 2014). The scattering from the TXD has therefore been measured at the same beamline using the SAXS set-up of the Helmholtz-Zentrum Berlin (HZB) (Gleber *et al.*, 2010). In Fig. 6, it is compared with the scattering from a thin SiN window and with a silicon-based TXD (Cruz *et al.*, 2015). Despite the much thicker substrate, the diamond TXD produces up to three orders of magnitude less scattering than the silicon-based device in the q-range below 0.1 nm^{-1}. However, it scatters more in the q-range above 0.1 nm^{-1}, which makes a reduced diamond thickness or a better surface finish desirable. The quadrant patterning of the diamond TXD produces strong artifacts which can be avoided by making use of sensor regions with uniform metallization.

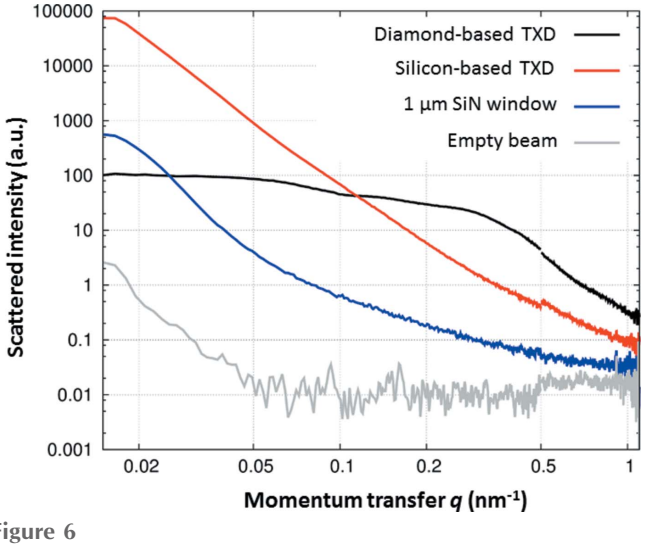

Figure 6
Scattered intensity (in arbitrary units, to allow direct comparison) of the diamond TXD compared with a silicon-based TXD and a thin SiN window.

6. Conclusion

Recent development of single-crystal diamond X-ray detectors has yielded devices with reliably linear and spatially uniform performance. Low dark current and low scattering at very small angles make these materials attractive for beam flux and position measurements. Quantitative flux measurements can be performed away from metallization gaps and plate edges. To further increase the transmittance, and thus the usable photon energy range towards lower photon energies, thinner diamond substrates and thinner platinum contacts would be beneficial. However, the quantitative analysis of transmittance and responsivity of the demonstrator TXD already provides a refinement of the mean electron–hole pair creation energy for diamond with very low uncertainty.

Acknowledgements

The authors thank Sydor Instruments and team for providing the demonstration unit and documentation (detector product SI-DBPM-M405V, article SN 015 here), as well as Christian Gollwitzer (PTB) for support during the SAXS measurements. This research is supported by the National Synchrotron Light Source II, a US Department of Energy (DOE) Office of Science User Facility operated for the DOE Office of Science by Brookhaven National Laboratory.

Funding information

The following funding is acknowledged: US Department of Energy, Office of Science (contract No. DE-SC0012704).

References

Almaviva, S., Marinelli, M., Milani, E., Prestopino, G., Tucciarone, A., Verona, C., Verona-Rinati, G., Angelone, M., Pillon, M., Dolbnya, I., Sawhney, K. & Tartoni, N. (2010). *J. Appl. Phys.* **107**, 014511.

Beckhoff, B., Gottwald, A., Klein, R., Krumrey, M., Müller, R., Richter, M., Scholze, F., Thornagel, R. & Ulm, G. (2009). *Phys. Status Solidi (b)*, **246**, 1415–1434.

Berdermann, E., Pomorski, M., de Boer, W., Ciobanu, M., Dunst, S., Grah, C., Kiš, M., Koenig, W., Lange, W., Lohmann, W., Lovrinčić, R., Moritz, P., Morse, J., Mueller, S., Pucci, A., Schreck, M., Rahman, S. & Träger, M. (2010). *Diamond Relat. Mater.* **19**, 358–367.

Berger, M. J., Hubbell, J. H., Seltzer, S. M., Chang, J., Coursey, J. S., Sukumar, R., Zucker, D. S. & Olsen, K. (2010). *XCOM: Photon Cross Section Database* (version 1.5). National Institute of Standards and Technology, Gaithersburg, MD, USA. https://www.nist.gov/pml/xcom-photon-cross-sections-database.

Bohon, J., Muller, E. & Smedley, J. (2010). *J. Synchrotron Rad.* **17**, 711–718.

Canali, C., Gatti, E., Kozlov, S. F., Manfredi, P. F., Manfredotti, C., Nava, F. & Quirini, A. (1979). *Nucl. Instrum. Methods*, **160**, 73–77.

Cruz, C., Jover-Manas, G., Matilla, O., Avila, J., Juanhuix, J., Pellegrini, G., Quirion, D. & Rodriguez, J. (2015). *J. Instrum.* **10**, C03005.
Desjardins, K., Pomorski, M. & Morse, J. (2014). *J. Synchrotron Rad.* **21**, 1217–1223.
Gaowei, M., Muller, E. M., Rumaiz, A. K., Weiland, C., Cockayne, E., Jordan-Sweet, J., Smedley, J. & Woicik, J. C. (2012). *Appl. Phys. Lett.* **100**, 201606.
Gerlach, M., Krumrey, M., Cibik, L., Müller, P., Rabus, H. & Ulm, G. (2008). *Metrologia*, **45**, 577–585.
Gleber, G., Cibik, L., Haas, S., Hoell, A., Müller, P. & Krumrey, M. (2010). *J. Phys. Conf. Ser.* **247**, 012027.
Hecht, K. (1932). *Z. Phys.* **77**, 235–245.
Hoell, A., Varga, Z., Raghuwanshi, V. S., Krumrey, M., Bocker, C. & Rüssel, C. (2014). *J. Appl. Cryst.* **47**, 60–66.
Hubbell, J. H. (1999). *Phys. Med. Biol.* **44**, R1–22.
Hubbell, J. H. & Seltzer, S. M. (2004). *Tables of X-ray Mass Attenuation Coefficients and Mass Energy-Absorption Coefficients* (version 1.4). National Institute of Standards and Technology, Gaithersburg, MD, USA. https://www.nist.gov/pml/x-ray-mass-attenuation-coefficients.
Keister, J. W. & Smedley, J. (2009). *Nucl. Instrum. Methods Phys. Res. A*, **606**, 774–779.
Keister, J. W., Smedley, J., Dimitrov, D. & Busby, R. (2010). *IEEE Trans. Nucl. Sci.* **57**, 2400–2404.
Kozlov, S. F., Stuck, R., Hage-Ali, M. & Siffert, P. (1975). *IEEE Trans. Nucl. Sci.* NS-**22**, 160–170.
Krumrey, M., Cibik, L. & Müller, P. (2010). *AIP Conf. Proc.* **1234**, 826–829.
Krumrey, M., Gerlach, M., Hoffmann, M. & Müller, P. (2007). *AIP Conf. Proc.* **879**, 1145–1147.
Krumrey, M. & Ulm, G. (2001). *Nucl. Instrum. Methods Phys. Res. A*, **467–468**, 1175–1178.
Morse, J., Salomé, M., Berdermann, E., Pomorski, M., Grant, J., O'Shea, V. & Ilinski, P. (2008). *MRS Symp. Proc.* **1039**, 1039-P06-02.
Muller, E. M., Gaowei, M., Ben-Zvi, I., Dimitrov, D. A. & Smedley, J. (2014). *Appl. Phys. Lett.* **104**, 093515.
Muller, E. M., Smedley, J., Bohon, J., Yang, X., Gaowei, M., Skinner, J., De Geronimo, G., Sullivan, M., Allaire, M., Keister, J. W., Berman, L. & Héroux, A. (2012). *J. Synchrotron Rad.* **19**, 381–387.
Muller, E. M., Smedley, J., Raghothamachar, B., Gaowei, M., Keister, J. W., Ben-Zvi, I., Dudley, M. & Wu, Q. (2010). *MRS Symp. Proc.* **1203**, 1203-J17-19.
Ravel, B., Attenkofer, K., Bohon, J., Muller, E. & Smedley, J. (2013). *Rev. Sci. Instrum.* **84**, 103106.
Varga, Z., Yuana, Y., Grootemaat, A. E., van der Pol, E., Gollwitzer, C., Krumrey, M. & Nieuwland, R. (2014). *J. Extracell. Vesicles*, **3**, 23298.